

CERN-EP-2022-188
15 September 2022

Measurement of the lifetime and Λ separation energy of ${}^3_{\Lambda}\text{H}$

ALICE Collaboration

Abstract

The most precise measurements to date of the ${}^3_{\Lambda}\text{H}$ lifetime τ and Λ separation energy B_{Λ} are obtained using the data sample of Pb–Pb collisions at $\sqrt{s_{\text{NN}}} = 5.02$ TeV collected by ALICE at the LHC. The ${}^3_{\Lambda}\text{H}$ is reconstructed via its charged two-body mesonic decay channel (${}^3_{\Lambda}\text{H} \rightarrow {}^3\text{He} + \pi^{-}$ and the charge-conjugate process). The measured values $\tau = [253 \pm 11 \text{ (stat.)} \pm 6 \text{ (syst.)}]$ ps and $B_{\Lambda} = [72 \pm 63 \text{ (stat.)} \pm 36 \text{ (syst.)}]$ keV are compatible with predictions from effective field theories and conclusively confirm that the ${}^3_{\Lambda}\text{H}$ is a weakly-bound system.

arXiv:2209.07360v1 [nucl-ex] 15 Sep 2022

Hypernuclei are bound states of nucleons and hyperons that are particularly interesting because they can be used as experimental probes for the study of the hyperon–nucleon (Y–N) interaction. Searching for hypernuclei and exploring the Y–N interaction have been a source of fascination for nuclear physicists since the discovery of the first hypernuclei in 1953 [1]. In recent years, measurements of the hypertriton production and lifetime have stimulated an interesting debate in the high-energy physics community. The knowledge of the Y–N interaction has become more relevant recently due to its connection to the modelling of dense astrophysical objects like neutron stars [2, 3]. Indeed, in the inner core of neutron stars the creation of hyperons is energetically favoured compared to purely nucleonic matter [4]. The presence of hyperons as additional degrees of freedom leads to a considerable modification of the matter equation of state (EOS), prohibiting the formation of high-mass neutron stars. This is incompatible with the observation of neutron stars heavier than two solar masses [2, 4], constituting what is referred to as the "hyperon puzzle". Many attempts were made to solve this puzzle, e.g. by introducing three-body forces leading to an additional repulsion that can counterbalance the large gravitational pressure and allow for larger star masses [5, 6]. To constrain the parameter space of such models, a detailed knowledge of the Y–N interaction and of the three-body Y–N–N interaction is mandatory, including Λ , Σ , and Ξ hyperons. Numerous particle correlation analyses [7, 8] directly contribute to the determination of such interactions. In a complementary approach, the lifetime and the binding energy of a hypernucleus reflect the strength of the Y–N interaction [9, 10]. The current estimate of the separation energy of the Λ in the hypertriton is $B_{\Lambda} = 181 \pm 48$ keV [11], which results in a RMS radius (average distance of the Λ to the deuteron) of the order of 10 fm [12–14]. Lower values (~ 90 keV) of B_{Λ} are favoured when fitting the correlation functions for protons and Λ baryons [15–17], therefore new measurements are required to understand this tension. The latest theoretical calculations predict a different degree of dependence of the ${}^3_{\Lambda}\text{H}$ lifetime on its binding energy. For pionless effective field theory (EFT) [18] based calculations, the ${}^3_{\Lambda}\text{H}$ lifetime is very close to the free Λ lifetime, with very little binding energy dependence for B_{Λ} values spanning from 0 to 0.5 MeV. On the other hand, in the χ EFT approach [19], a stronger dependence on the binding energy is predicted for the ${}^3_{\Lambda}\text{H}$ lifetime being $\tau = (163 \pm 18)$ ps for $B_{\Lambda} = 410$ keV and $\tau = (234 \pm 27)$ ps for $B_{\Lambda} = 69$ keV. Previous measurements of the lifetime [20–25] and B_{Λ} [26] of ${}^3_{\Lambda}\text{H}$ in heavy-ion collisions have still quite large uncertainties. In this letter, new measurements with unprecedented precision of the ${}^3_{\Lambda}\text{H}$ lifetime and binding energy are presented to address the questions about its structure.

The presented results are based on data collected during the 2018 Pb–Pb LHC run at a centre-of-mass energy per nucleon pair of $\sqrt{s_{\text{NN}}} = 5.02$ TeV. The ALICE detector and its performance are described in detail in Refs. [27, 28]. Events are selected by using the information from the V0A and V0C scintillator arrays [29], located on both sides of the interaction point, covering the pseudorapidity intervals $2.8 < \eta < 5.1$ and $-3.7 < \eta < -1.7$, respectively. A coincidence of signals in both arrays is used as a minimum-bias trigger. In addition, two thresholds on the minimum amount of charge deposited on the V0 detector are employed to trigger on central and semi-central Pb–Pb collisions. Only events with the primary vertex position within 10 cm along the beam axis relative to the nominal centre of the experiment are selected offline to benefit from the full acceptance of the detector. The 90% most central collisions are chosen in this analysis using a centrality estimator based on the V0 detector arrays [30]. The centrality distribution of the selected events reflects the three different triggers employed. Furthermore, Pb–Pb collisions with more than one reconstructed primary interaction vertex (pile-up events) are rejected to avoid ambiguous associations of ${}^3_{\Lambda}\text{H}$ candidates to their production vertices. In total, about 300 million events are selected for this analysis.

In Pb–Pb collisions at the LHC, approximately the same number of ${}^3_{\Lambda}\text{H}$ and ${}^3_{\Lambda}\bar{\text{H}}$ are expected to be produced. The ${}^3_{\Lambda}\text{H}$ candidates are reconstructed via the charged two-body decay channel ${}^3_{\Lambda}\text{H} \rightarrow {}^3\text{He} + \pi^{-}$ (and the corresponding charge-conjugated particles for ${}^3_{\Lambda}\bar{\text{H}}$). The charged particle tracks are reconstructed in the ALICE central barrel with the Inner Tracking System [31] and the Time Projection Chamber (TPC) [32], which are located within a solenoid that provides a homogeneous magnetic field of 0.5 T

in the direction of the beam axis. These two subsystems provide full azimuthal coverage for charged particle trajectories in the pseudorapidity interval $|\eta| < 0.8$. The TPC is also used for the particle identification (PID) of the ${}^3\text{He}$, the π^- , and their charge conjugates via their specific energy loss dE/dx in the gas volume, with a dE/dx resolution of about 5% [32, 33]. The $n(\sigma_i^{\text{TPC}})$ variable represents the PID response in the TPC expressed in terms of the deviation between the measured and the expected dE/dx for a particle species i , in units of the detector resolution σ . The expected dE/dx is computed with a parameterised Bethe–Bloch function [28]. Pion and ${}^3\text{He}$ tracks within $\pm 5\sigma^{\text{TPC}}$ are selected.

The identified ${}^3\text{He}$ and π tracks are then used to reconstruct the ${}^3_{\Lambda}\text{H}$ weak-decay topology with an algorithm similar to the one employed in previous analyses [22, 24, 34]. By combining the information on the decay kinematics and decay vertex, several selection variables are defined. Those used in the analysis are: the distance of closest approach both from the primary and the decay vertex and the $n(\sigma_i^{\text{TPC}})$ of each daughter track, the number of clusters of the ${}^3\text{He}$ track in the TPC, the reconstructed p_T of the ${}^3_{\Lambda}\text{H}$, and $\cos(\theta_p)$, where θ_p is the angle between the total momentum vector of the decay daughters and the straight line connecting the primary and secondary vertices. The final candidate selection based on these variables is performed with a gradient-boosted decision tree classifier (BDT) implemented by the XGBOOST library [35, 36] and trained on a dedicated Monte Carlo (MC) simulated event sample. The MC sample is created using the HIJING event generator [37] for simulating the underlying Pb–Pb collisions, while ${}^3_{\Lambda}\text{H}$ signals are injected with a transverse momentum (p_T) distribution given by the blast-wave [38] function, with parameters taken from simultaneous fits of the p_T distribution of light-flavoured hadrons measured in Pb–Pb collisions [39]. The particles are transported through the detector geometry using GEANT4 [40], which simulates the interaction with the material and the weak decay of the ${}^3_{\Lambda}\text{H}$. The BDT is a supervised learning algorithm that determines how to discriminate between two or more classes, in this case signal and background, by examining sets of examples called the training sets. In this analysis, the training sets are composed of ${}^3_{\Lambda}\text{H}$ signal candidates extracted from the MC sample and background candidates from paired like-sign ${}^3\text{He}$ and π tracks from data. For each ${}^3_{\Lambda}\text{H}$ candidate, the BDT combines topological and single-track variables to return a score, which is used to discriminate between signal or background. In particular, the most important variable employed by the BDT for the classification is the $\cos(\theta_p)$. The selection is based on the BDT score, defining a threshold that maximises the expected signal significance assuming a production yield as predicted by the thermal statistical hadronization model [12] for the ${}^3_{\Lambda}\text{H}$ and the background rate observed when combining like-sign ${}^3\text{He}$ and π pairs.

The sample of ${}^3_{\Lambda}\bar{\text{H}}$ and ${}^3_{\Lambda}\text{H}$ candidates is divided into nine $ct = ML/p$ intervals, where c is the speed of light, t is the proper time of the candidate, M is the mass of the candidate, L is the decay distance, and p is the reconstructed momentum. The BDT training and threshold optimisation is repeated for each ct interval. The candidates that pass the BDT selection are used to populate the invariant-mass distribution, as shown in Fig. 1. An unbinned maximum-likelihood fit is performed on the invariant-mass distribution using a Kernel Density Estimator (KDE) function [41, 42], constructed using the MC sample to describe the signal and a linear function to describe the background. An example is shown in Fig. 1. The KDE is used to model the non-Gaussian behaviour of the signal shape observed in the simulation by means of a superposition of Gaussian functions. The widths of the Gaussian functions are determined with an adaptive procedure that takes into account the local density of the signal in the MC.

The ${}^3_{\Lambda}\text{H}$ lifetime is extracted by fitting the corrected ct spectrum with an exponential function. The yield in each ct interval is obtained from the fit to the invariant-mass spectrum. The fitted signal is corrected for the reconstruction and selection efficiency, and for the acceptance of the ALICE detector. The inelastic interactions and the energy loss of the daughter particles are simulated with GEANT4 and are taken into account in the reconstruction efficiency computation. According to Ref. [43], the expected absorption cross section of ${}^3_{\Lambda}\text{H}$ due to the inelastic interactions in the ALICE detector material is about 1.5 times that of ${}^3\text{He}$ ($\sigma_{\text{inel}}^{{}^3\text{He}}$). This value is used for simulating the passage of ${}^3_{\Lambda}\text{H}$ in the detector and evaluating the effect on the reconstruction efficiency. The typical total efficiency (including acceptance, reconstruction,

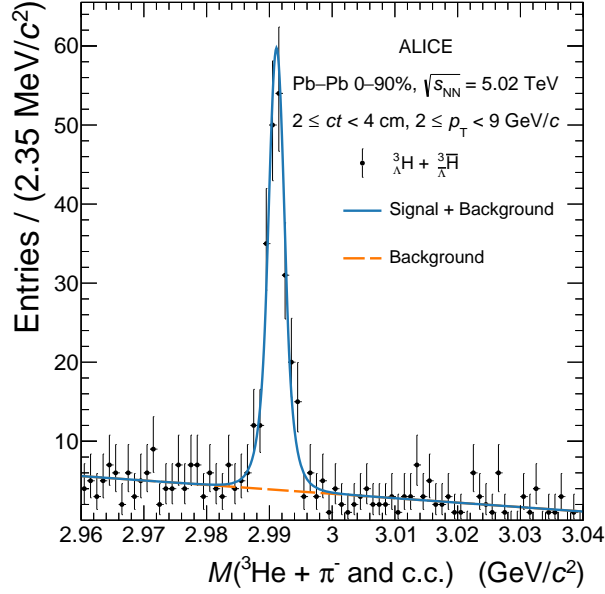


Figure 1: Invariant-mass distribution of the selected ${}^3\text{He} + \pi^-$ and charge conjugate pairs. Vertical lines represent the statistical Poisson-distributed uncertainties. A two component model is fitted to the invariant-mass spectrum: the blue line represents the total fit while the orange dashed line shows the background component only.

and selection) is around 15% while, the absorption probability of ${}^3_\Lambda\text{H}$ due to the inelastic interactions in the ALICE detector material is of the order of few percent.

The systematic uncertainties originate from (1) the ${}^3_\Lambda\text{H}$ selection and the signal extraction and, (2) the uncertainty on the ${}^3_\Lambda\text{H}$ absorption in the detector. The total uncertainty is obtained as the quadratic sum of the individual contributions. The first contribution, which is the dominant one, is computed by varying simultaneously the BDT threshold ($\pm 5\%$), the background fit function (constant, linear, and exponential) and the signal (KDE and double sided Crystal Ball [44]) fit functions in each ct interval. The systematic uncertainty is given by the RMS of the distribution of lifetimes obtained from 5×10^4 different combinations and amounts to approximately 2%. The second contribution is evaluated by varying the ${}^3_\Lambda\text{H}$ absorption cross section and evaluating the effect on the lifetime. The systematic uncertainty due to the assumption on the ${}^3_\Lambda\text{H}$ absorption cross section is evaluated by employing different cross sections for the ${}^3_\Lambda\text{H}$ from zero (no interaction) to $2\sigma_{\text{inel}}^{3\text{He}}$. For each variation the lifetime is recalculated, resulting in a systematic uncertainty of 1%.

The Λ separation energy B_Λ is obtained in each ct interval using the ${}^3_\Lambda\text{H}$ mass extracted from the fit ($\mu_{3_\Lambda\text{H}}$), the deuteron mass taken from CODATA [45], and the Λ mass taken from the PDG [46]. The reconstructed value of $\mu_{3_\Lambda\text{H}}$ is affected by the imperfect correction for the energy loss of the daughter particles in the ALICE material. This effect produces a shift that depends on the decay radius of the ${}^3_\Lambda\text{H}$ candidates and whose value is evaluated by analysing the MC simulations (δ_{MC}). To account for the possible mismatch between data and simulation, an additional data-driven correction is applied which is based on a dedicated new precise measurement of the Λ mass. This represents an ideal test for the full analysis chain and for a potential data–simulation mismatch since the Λ mass is known with a precision of 6 keV [46] and its lifetime is compatible within 1σ with the ${}^3_\Lambda\text{H}$ one. Hence, the Λ mass is computed with the same analysis procedure employed for the ${}^3_\Lambda\text{H}$, and the shift obtained with respect to the PDG value ($\delta_\Lambda \sim 30$ keV) is used as our estimate of data–simulation mismatch and for correcting our value of $\mu_{3_\Lambda\text{H}}$. Finally, in each ct interval B_Λ is computed as $B_\Lambda = m_d + m_\Lambda - (\mu_{3_\Lambda\text{H}} - \delta_{\text{MC}} - \delta_\Lambda)$. As shown in Fig. 2, the final B_Λ value and its statistical uncertainty are obtained from the average of the values measured in each ct interval weighted on their statistical uncertainties.

The systematic uncertainties on B_Λ originate from (1) the ${}^3_\Lambda\text{H}$ selection and the signal extraction, (2) the uncertainty on δ_Λ , and (3) the uncertainty on the ALICE material budget. The first contribution is computed using the same method as for the lifetime analysis and amounts to ± 33 keV. The uncertainty on δ_Λ takes into account a 13 keV shift observed by repeating the Λ mass measurement with standard linear selections. Finally, the systematic contribution due to the uncertainty on the ALICE material budget is computed by varying the material budget in the MC by its uncertainty and repeating the analysis. For each variation the B_Λ is recomputed resulting in a systematic uncertainty of 8 keV. The systematic uncertainty is taken as the sum in quadrature of the three contributions. For both the determination of the mean lifetime of the ${}^3_\Lambda\text{H}$ and its B_Λ , the contribution from the knowledge of the magnetic field is considered by performing the analysis separately for positive and negative polarities of the solenoidal magnet. As the analyses with the two polarities returned results statistically compatible with each other, no further systematic uncertainty is added.

For both the lifetime and the B_Λ analyses, other potential sources of systematic uncertainty were tested such as the input p_T and ct shape of ${}^3_\Lambda\text{H}$ in the Monte Carlo sample, the BDT hyperparameters, the discrepancy between BDT and linear selections, and the ${}^3_\Lambda\text{H}$ reconstruction algorithm, all resulting in a non-significant contribution.

The measurements for the ${}^3_\Lambda\text{H}$ and ${}^3_{\bar{\Lambda}}\text{H}$ lifetime and B_Λ obtained with this analysis are

$$\tau = [253 \pm 11 \text{ (stat.)} \pm 6 \text{ (syst.)}] \text{ ps},$$

$$B_\Lambda = [72 \pm 63 \text{ (stat.)} \pm 36 \text{ (syst.)}] \text{ keV}.$$

As shown in Fig. 3, the measurements are in agreement with both the predictions from pionless EFT [18] and from χEFT [19], while they severely restrict the phase space available for these theories and strongly confirm the weakly-bound nature of ${}^3_\Lambda\text{H}$. Furthermore, the new measurement of the B_Λ is in agreement within 1σ with the binding energy value describing best the p - Λ correlations measured with the femtoscopy technique [16, 17].

Finally, the difference between the ${}^3_\Lambda\text{H}$ and ${}^3_{\bar{\Lambda}}\text{H}$ lifetimes is measured, giving the value

$$\tau_{{}^3_\Lambda\text{H}} - \tau_{{}^3_{\bar{\Lambda}}\text{H}} = [2 \pm 19 \text{ (stat.)} \pm 11 \text{ (syst.)}] \text{ ps},$$

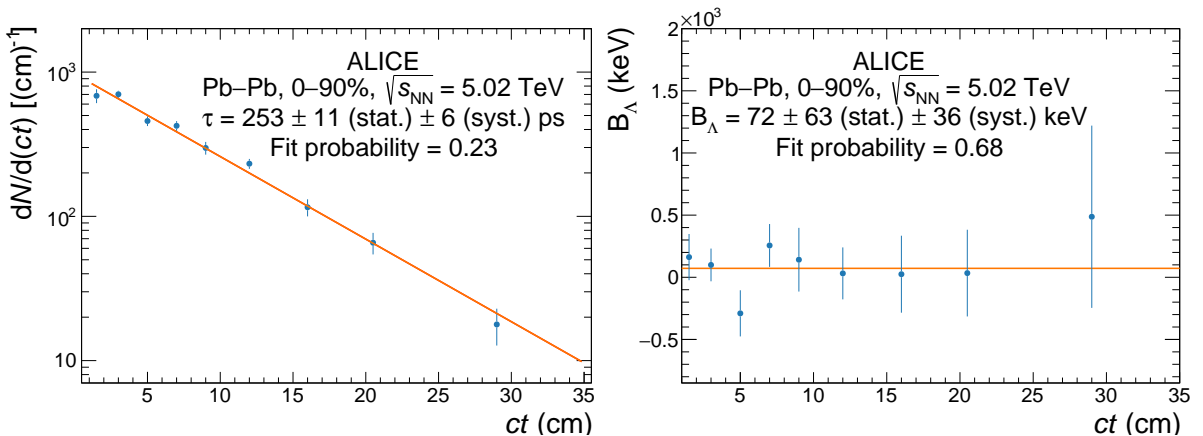


Figure 2: Left: exponential decay spectrum as a function of the proper decay length for ${}^3_\Lambda\text{H}$, the blue points represent the measured yield, while the orange line represents the best fit to the measurement. Right: B_Λ measurement as a function of the proper decay length. Only statistical uncertainties are shown, see the text for a description of the determination of the systematic uncertainties. The fit probability computed with a Pearson test is reported.

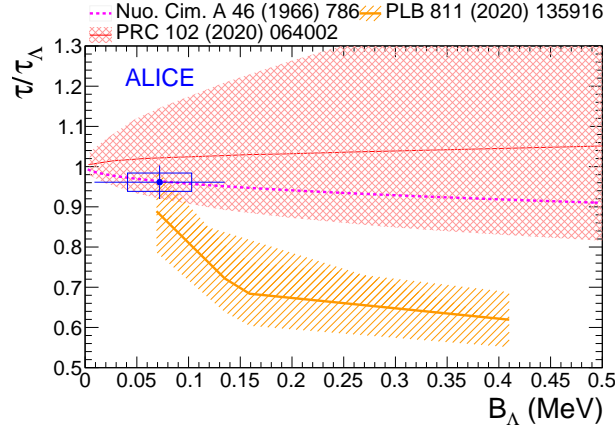


Figure 3: The ${}^3_\Lambda\text{H}$ lifetime relative to the free Λ lifetime as a function of the B_Λ for pionless EFT [18] (red), χ EFT [19] (orange), and the original π exchange calculations [47] (magenta). The blue point represents the measurement presented in this Letter with the statistical and systematic uncertainties depicted with lines and box, respectively.

which is consistent with zero, and therefore with the CPT symmetry expectation, within uncertainties.

In summary, the most precise measurements to date of the ${}^3_\Lambda\text{H}$ lifetime and B_Λ , presented in this Letter, strongly support the loosely-bound nature of ${}^3_\Lambda\text{H}$ and contribute significantly to the understanding of the Y - N interaction. The measured value is indeed in perfect agreement with the B_Λ that fits best the correlation functions for protons and Λ baryons [15–17]. The main remaining piece to be set for the complete understanding of the ${}^3_\Lambda\text{H}$ structure is the measurement of branching ratios for the various decay channels [18]. The Run 3 of the LHC will make those measurements accessible with unprecedented precision.

References

- [1] M. Danysz and J. Pniewski, “Delayed disintegration of a heavy nuclear fragment: I”, *The London, Edinburgh, and Dublin Philosophical Magazine and Journal of Science* **44** no. 350, (1953) 348–350.
- [2] J. Schaffner-Bielich, *Neutron Stars*, p. 147–208. Cambridge University Press, 2020.
- [3] J. M. Lattimer and M. Prakash, “The physics of neutron stars”, *Science* **304** (2004) 536–542, arXiv:astro-ph/0405262.
- [4] L. Tolos and L. Fabbietti, “Strangeness in Nuclei and Neutron Stars”, *Prog. Part. Nucl. Phys.* **112** (2020) 103770, arXiv:2002.09223 [nucl-ex].
- [5] D. Lonardonì, A. Lovato, S. Gandolfi, and F. Pederiva, “Hyperon Puzzle: Hints from Quantum Monte Carlo Calculations”, *Phys. Rev. Lett.* **114** no. 9, (2015) 092301, arXiv:1407.4448 [nucl-th].
- [6] D. Logoteta, I. Vidana, and I. Bombaci, “Impact of chiral hyperonic three-body forces on neutron stars”, *Eur. Phys. J. A* **55** no. 11, (2019) 207, arXiv:1906.11722 [nucl-th].
- [7] L. Fabbietti, V. Mantovani Sarti, and O. Vazquez Doce, “Study of the Strong Interaction Among Hadrons with Correlations at the LHC”, *Ann. Rev. Nucl. Part. Sci.* **71** (2021) 377–402, arXiv:2012.09806 [nucl-ex].

- [8] **ALICE** Collaboration, S. Acharya *et al.*, “Unveiling the strong interaction among hadrons at the LHC”, *Nature* **588** (2020) 232–238, arXiv:2005.11495 [nucl-ex]. [Erratum: *Nature* **590** (2021) E13].
- [9] R. H. Dalitz and G. Rajasekharan, “The spins and lifetimes of the light hypernuclei”, *Phys. Lett.* **1** (1962) 58–60.
- [10] H. Kamada, J. Golak, K. Miyagawa, H. Witala, and W. Gloeckle, “Pi mesonic decay of the hypertriton”, *Phys. Rev. C* **57** (1998) 1595–1603, arXiv:nucl-th/9709035.
- [11] P. Eckert, P. Achenbach, *et al.*, “Chart of hypernuclides — Hypernuclear structure and decay data”, 2021. <https://hypernuclei.kph.uni-mainz.de>.
- [12] P. Braun-Munzinger and B. Dönigus, “Loosely-bound objects produced in nuclear collisions at the LHC”, *Nucl. Phys. A* **987** (2019) 144–201, arXiv:1809.04681 [nucl-ex].
- [13] A. Gal and H. Garcilazo, “Towards resolving the ${}^3_{\Lambda}\text{H}$ lifetime puzzle”, *Phys. Lett. B* **791** (2019) 48–53, arXiv:1811.03842 [nucl-th].
- [14] F. Hildenbrand and H. W. Hammer, “Three-Body Hypernuclei in Pionless Effective Field Theory”, *Phys. Rev. C* **100** no. 3, (2019) 034002, arXiv:1904.05818 [nucl-th]. [Erratum: *Phys. Rev. C* **102**, (2020) 039901].
- [15] **ALICE** Collaboration, S. Acharya *et al.*, “p-p, p- Λ and Λ - Λ correlations studied via femtoscopy in pp reactions at $\sqrt{s} = 7$ TeV”, *Phys. Rev. C* **99** no. 2, (2019) 024001, arXiv:1805.12455 [nucl-ex].
- [16] J. Haidenbauer, U. G. Meißner, and A. Nogga, “Hyperon–nucleon interaction within chiral effective field theory revisited”, *Eur. Phys. J. A* **56** no. 3, (2020) 91, arXiv:1906.11681 [nucl-th].
- [17] **ALICE** Collaboration, S. Acharya *et al.*, “Exploring the $\text{N}\Lambda$ - $\text{N}\Sigma$ coupled system with high precision correlation techniques at the LHC”, *Phys. Lett. B* **833** (2022) 137272, arXiv:2104.04427 [nucl-ex].
- [18] F. Hildenbrand and H. W. Hammer, “Lifetime of the hypertriton”, *Phys. Rev. C* **102** (2020) 064002, arXiv:2007.10122 [nucl-th].
- [19] A. Pérez-Obiol, D. Gazda, E. Friedman, and A. Gal, “Revisiting the hypertriton lifetime puzzle”, *Phys. Lett. B* **811** (2020) 135916, arXiv:2006.16718 [nucl-th].
- [20] **STAR** Collaboration, B. I. Abelev *et al.*, “Observation of an Antimatter Hypernucleus”, *Science* **328** (2010) 58–62, arXiv:1003.2030 [nucl-ex].
- [21] C. Rappold *et al.*, “Hypernuclear spectroscopy of products from ${}^6\text{Li}$ projectiles on a carbon target at 2 AGeV”, *Nucl. Phys. A* **913** (2013) 170–184, arXiv:1305.4871 [nucl-ex].
- [22] **ALICE** Collaboration, J. Adam *et al.*, “ ${}^3_{\Lambda}\text{H}$ and ${}^3_{\Lambda}\bar{\text{H}}$ production in Pb-Pb collisions at $\sqrt{s_{\text{NN}}} = 2.76$ TeV”, *Phys. Lett. B* **754** (2016) 360–372, arXiv:1506.08453 [nucl-ex].
- [23] **STAR** Collaboration, L. Adamczyk *et al.*, “Measurement of the ${}^3_{\Lambda}\text{H}$ lifetime in Au+Au collisions at the BNL Relativistic Heavy Ion Collider”, *Phys. Rev. C* **97** no. 5, (2018) 054909, arXiv:1710.00436 [nucl-ex].
- [24] **ALICE** Collaboration, S. Acharya *et al.*, “ ${}^3_{\Lambda}\text{H}$ and ${}^3_{\Lambda}\bar{\text{H}}$ lifetime measurement in Pb-Pb collisions at $\sqrt{s_{\text{NN}}} = 5.02$ TeV via two-body decay”, *Phys. Lett. B* **797** (2019) 134905, arXiv:1907.06906 [nucl-ex].

- [25] **STAR** Collaboration, M. Abdallah *et al.*, “Measurements of HA3 and HA4 Lifetimes and Yields in Au+Au Collisions in the High Baryon Density Region”, *Phys. Rev. Lett.* **128** no. 20, (2022) 202301, arXiv:2110.09513 [nucl-ex].
- [26] **STAR** Collaboration, J. Adam *et al.*, “Measurement of the mass difference and the binding energy of the hypertriton and antihypertriton”, *Nature Phys.* **16** no. 4, (2020) 409–412, arXiv:1904.10520 [hep-ex].
- [27] **ALICE** Collaboration, K. Aamodt *et al.*, “The ALICE experiment at the CERN LHC”, *JINST* **3** (2008) S08002.
- [28] **ALICE** Collaboration, B. Abelev *et al.*, “Performance of the ALICE Experiment at the CERN LHC”, *Int. J. Mod. Phys. A* **29** (2014) 1430044, arXiv:1402.4476 [nucl-ex].
- [29] **ALICE** Collaboration, E. Abbas *et al.*, “Performance of the ALICE VZERO system”, *JINST* **8** (2013) P10016, arXiv:1306.3130 [nucl-ex].
- [30] **ALICE** Collaboration, “Centrality determination in heavy ion collisions”, *ALICE-PUBLIC-2018-011* (2018). <https://cds.cern.ch/record/2636623>.
- [31] **ALICE** Collaboration, K. Aamodt *et al.*, “Alignment of the ALICE Inner Tracking System with cosmic-ray tracks”, *JINST* **5** (2010) P03003, arXiv:1001.0502 [physics.ins-det].
- [32] J. Alme *et al.*, “The ALICE TPC, a large 3-dimensional tracking device with fast readout for ultra-high multiplicity events”, *Nucl. Instrum. Meth. A* **622** (2010) 316–367, arXiv:1001.1950 [physics.ins-det].
- [33] **ALICE** Collaboration, B. B. Abelev *et al.*, “Production of charged pions, kaons and protons at large transverse momenta in pp and Pb–Pb collisions at $\sqrt{s_{\text{NN}}}=2.76$ TeV”, *Phys. Lett. B* **736** (2014) 196–207, arXiv:1401.1250 [nucl-ex].
- [34] **ALICE** Collaboration, S. Acharya *et al.*, “Hypertriton Production in p-Pb Collisions at $\sqrt{s_{\text{NN}}}=5.02$ TeV”, *Phys. Rev. Lett.* **128** no. 25, (2022) 252003, arXiv:2107.10627 [nucl-ex].
- [35] T. Chen and C. Guestrin, “Xgboost: A scalable tree boosting system”, in *Proceedings of the 22nd ACM SIGKDD International Conference on Knowledge Discovery and Data Mining, KDD ’16*, p. 785–794. Association for Computing Machinery, New York, NY, USA, 2016. <https://doi.org/10.1145/2939672.2939785>.
- [36] L. Barioglio, F. Catalano, M. Concas, P. Fecchio, F. Grosa, F. Mazzaschi, and M. Puccio, “hipe4ml/hipe4ml”, Nov., 2021. <https://doi.org/10.5281/zenodo.5734093>.
- [37] X.-N. Wang and M. Gyulassy, “HIJING: A Monte Carlo model for multiple jet production in pp, pA and AA collisions”, *Phys. Rev. D* **44** (1991) 3501–3516.
- [38] E. Schnedermann, J. Sollfrank, and U. W. Heinz, “Thermal phenomenology of hadrons from 200-A/GeV S+S collisions”, *Phys. Rev. C* **48** (1993) 2462–2475, arXiv:nucl-th/9307020.
- [39] **ALICE** Collaboration, S. Acharya *et al.*, “Production of charged pions, kaons, and (anti-)protons in Pb-Pb and inelastic pp collisions at $\sqrt{s_{\text{NN}}}=5.02$ TeV”, *Phys. Rev. C* **101** no. 4, (2020) 044907, arXiv:1910.07678 [nucl-ex].
- [40] **GEANT4** Collaboration, S. Agostinelli *et al.*, “GEANT4—a simulation toolkit”, *Nucl. Instrum. Meth. A* **506** (2003) 250–303.

- [41] K. S. Cranmer, “Kernel estimation in high-energy physics”, *Comput. Phys. Commun.* **136** (2001) 198–207, arXiv:hep-ex/0011057.
- [42] W. Verkerke and D. P. Kirkby, “The RooFit toolkit for data modeling”, *eConf C0303241* (2003) MOLT007, arXiv:physics/0306116.
- [43] M. V. Evlanov, A. M. Sokolov, V. K. Tartakovsky, S. A. Khorozov, and Y. Lukstins, “Interaction of hypertritons with nuclei at high-energies”, *Nucl. Phys. A* **632** (1998) 624–632.
- [44] **ALICE collaboration** Collaboration, “Quarkonium signal extraction in ALICE”, *ALICE-PUBLIC-2015-006* (2015) . <https://cds.cern.ch/record/2060096>.
- [45] P. J. Mohr, D. B. Newell, and B. N. Taylor, “CODATA Recommended Values of the Fundamental Physical Constants: 2014”, *Rev. Mod. Phys.* **88** no. 3, (2016) 035009, arXiv:1507.07956 [physics.atom-ph].
- [46] **Particle Data Group** Collaboration, P. Zyla *et al.*, “Review of Particle Physics”, *PTEP* **2020** no. 8, (2020) 083C01.
- [47] M. Rayet and R. H. Dalitz, “Lifetime of H-3”, *Nuovo Cim. A* **46** (1966) 786–794.

A Additional Material

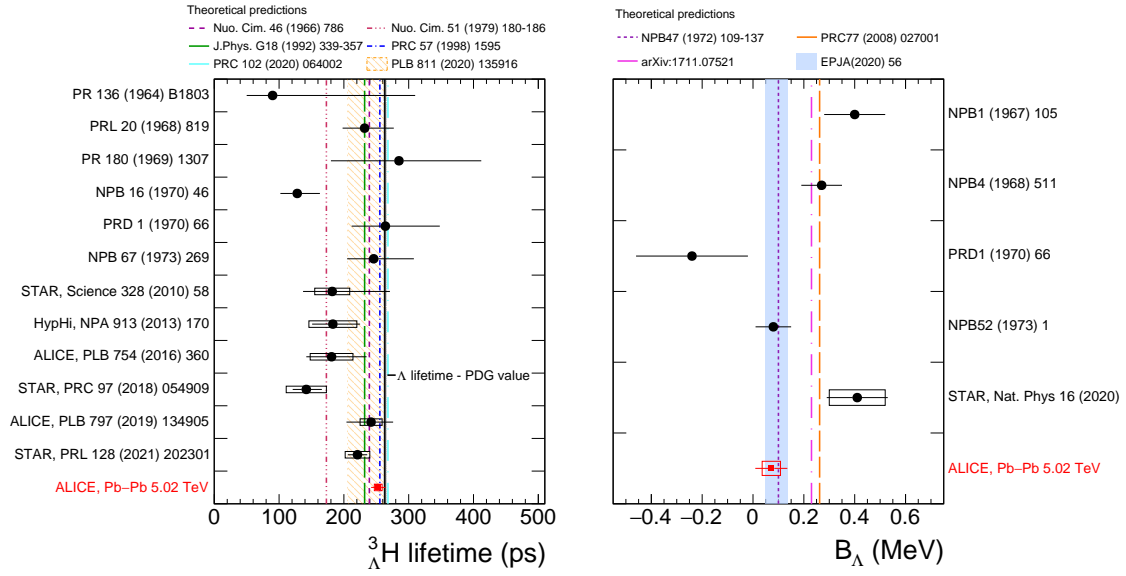


Figure A.1: Collection of the ${}^3_\Lambda\text{H}$ lifetime (left) and B_Λ (right) measurements obtained with different experimental techniques. The horizontal lines and boxes are the statistical and systematic uncertainties respectively. The dashed-dotted lines are the corresponding theoretical predictions.